A compact and fully integrated 0.48 THz FMCW radar transceiver combined with a dielectric lens

David Starke[1] , Jonathan Bott[1] , Florian Vogelsang[1] , Benedikt Sievert[2] , Jan Barowski[3] , Christian Schulz[3] , Holger Rücker[4] , Andreas Rennings[2] , Daniel Erni[2] , Ilona Rolfes[3] and Nils Pohl[1,5]

[1]Institute of Integrated Systems, Ruhr University Bochum, Bochum, Germany ; [2]General and Theoretical Electrical Engineering (ATE), University of Duisburg-Essen, and CENIDE – Center for Nanointegration Duisburg-Essen, Duisburg, Germany; [3]Institute of Microwave Systems, Ruhr University Bochum, Bochum, Germany; [4]IHP – Leibniz-Institut für innovative Mikroelektronik, Frankfurt (Oder), Germany and [5]Fraunhofer Institute for High Frequency Physics and Radar Techniques FHR, Wachtberg, Germany

Abstract

Electronic measurement systems in the THz frequency range are often bulky and expensive devices. While some compact single-chip systems operating in the high millimeter-wave frequency range have recently been published, compact measurement systems in the low THz frequency range are still rare. The emergence of new silicon-germanium (SiGe) semiconductor technologies allow the integration of system components, like oscillators, frequency multipliers, frequency dividers, and antennas, operating in the low THz frequency range, into a compact monolithic microwave integrated circuits (MMIC), which contains most components to implement a low-cost and compact frequency-modulated continuous-wave-radar transceiver. This article presents a single transceiver solution containing all necessary components. It introduces a 0.48 THz radar transceiver MMIC with a tuning range of 43 GHz and an output power of up to −9.4 dBm in the SG13G3 130 nm SiGe technology by IHP. The MMIC is complemented by a dielectric lens antenna design consisting of polytetrafluoroethylene, providing up to 39.3 dBi of directivity and half-power beam widths of 0.95° in transmit and receive direction. The suppression of clutter from unwanted targets deviating from antenna boresight more than 6° is higher than 24.6 dB in E- and H-Plane.

Introduction

The upper millimeter-wave and THz frequency ranges are interesting for multiple applications, like material characterization and localization, medical applications, and non-destructive testing [1–5]. This frequency range is not only of importance because of the large available bandwidth, but also because of the high center frequency, as unique material fingerprints often occur in the THz range [6]. Furthermore, the high operating frequency enables the implementation of fully integrated measurement systems because of the possibility of integrating the antennas on the monolithic microwave integrated circuits (MMIC) due to the small wavelength at these frequencies. Millimeter-wave and THz frequencies enable smaller package sizes and a higher channel count in MIMO and phased-array applications and, therefore, a higher lateral resolution [7].

There are also challenges associated with the high frequency of these systems. Due to the limited availability of THz-ready semiconductor technologies, designing circuits targeting this frequency range is challenging, as many circuits operate at or above the transistors' transit frequencies. Therefore, the transmitter's radiated power, as well as the receiver's conversion gain is often limited. Furthermore, due to the high losses of bond interconnections [8], integrated antennas are the primary method of interfacing the THz circuits with the environment. These antennas typically have low bandwidth and efficiencies because of the small distance between the radiating element and the ground plane of the MMIC [9].

In recent years, many millimeter-wave [10, 11] and especially THz [12–17] transceivers and systems based on silicon-germanium (SiGe) technologies have been published. While III–V-based systems can provide high output power [18–20], demand for silicon-based systems is driven by low manufacturing cost and overall compactness, which are vital for widespread deployment [21].

A commonly used approach to improve the measurement range of millimeter-wave and THz systems is the usage of dielectric lenses [22–25]. These lenses narrow the beam of the on-chip
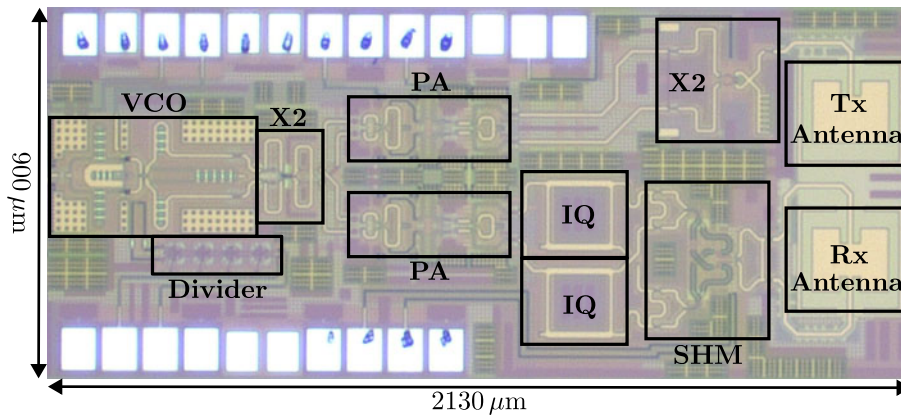
CAMBRIDGE
UNIVERSITY PRESS

Figure 1. Photograph of the developed transceiver MMIC. The signal generation up to 240 GHz is depicted on the left of the figure(VCO, X2, Divider). On the top right, the transmit path is shown (PA, X2, Tx Antenna). The receive path can be seen on the bottom right (PA, IQ, SHM, Rx Antenna). This highly integrated 0.48 THz transceiver is realized on an MMIC with an area of just $1.92\,mm^2$.

antennas for improved antenna directivity and measurement range as well as suppression of unwanted targets.

An earlier version of this paper was presented at the European Microwave Integrated Circuits Conference (EuMIC) 2022 and was published in its Proceedings [26]. This paper expands the previous publication by complementing the published on-chip antennas with a dielectric lens design with high directivity, enabling higher measurement ranges and suppression of clutter from unwanted targets.

In this article, we start by detailing the system concept of the proposed radar sensor in Section "System concept". Section "MMIC design" presents the building blocks of the developed MMIC, including the measurement results of the circuits. The dielectric lens design, complementing the developed radar MMIC, is shown in Section "Dielectric lens antenna". After a brief comparison of the proposed THz transceiver system to the state of the art in electronic THz transceiver design in Section "Comparison to state-of-the-art electronic THz transceivers", the article is concluded in Section "Conclusion".

System concept

In this paper, a concept for a low-cost THz frequency-modulated continuous-wave (FMCW) radar sensor is presented, that is based on a fully integrated FMCW 0.48 THz radar transceiver MMIC [26] and a dielectric lens for antenna directivity and measurement range improvements.

A block diagram of the presented MMIC architecture is depicted in Fig. 2. A photograph of the manufactured MMIC is shown in Fig. 1. The circuit blocks previously described are shown in an overlay on the micrograph. The MMIC's dimensions are 2130 μm by 900 μm with a power consumption of 877 mW at a supply voltage of 3.3 V.

In contrast to other FMCW radar sensors in the sub-THz and THz spectrum, which use external signal generation [13, 17, 27–30], we developed a fully integrated sensor. The frequency stabilization and chirp generation, performed by a phase-locked loop (PLL), were omitted from the fully integrated approach for several reasons. A fully programmable PLL design would have added a tremendous amount of complexity to the MMIC design and would have to be based on the simulation results of the oscillator. Furthermore, the loop filter of an integrated PLL would need to be placed on the frontend PCB due to the large component values. Hence, an external PLL on the front end is much more flexible, as it can be optimized after fabrication and measurement
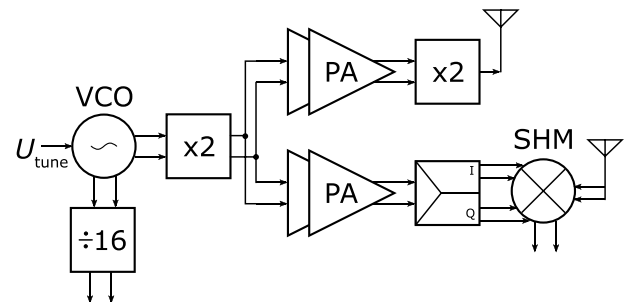

Figure 2. Block diagram of the developed transceiver MMIC.

of the radar MMIC. An integrated voltage-controlled oscillator (VCO) at a quarter of the targeted output frequency of 480 GHz generates the LO signal and can be tuned to modulate the output frequency.

For frequency stabilization by the PLL, a by-16 frequency divider lowers the 120 GHz output signal of the VCO down to approx. 7.5 GHz which, allows the use of commercial PLL components [31].

A Gilbert-cell-based frequency doubler doubles the oscillator's frequency before the signal is split into the transmit (Tx) and receive (Rx) path. A bistatic approach was chosen for this radar MMIC as it relaxes the requirements regarding the receive mixer, as there is no direct coupling from the Tx into the Rx path, as no directional coupler is used between the transmitter and receiver. In both paths, the signal is amplified by power amplifiers (PAs) to drive the subsequent building blocks of the transceiver.

The Tx signal is frequency doubled again by a push–push frequency doubler that creates the 0.48 THz output signal. As push-push doublers convert a differential input signal to a single-ended output signal, a single-ended patch antenna is used as Tx antenna.

In the Rx path, the amplified signal at half of the output frequency is converted to quadrature signals by microstrip-based branchline couplers (IQ) and then used to drive a subharmonic down-conversion mixer (SHM). As the subharmonic mixer has a differential RF input, a differential patch antenna can be used for signal reception.

As the signal generation of this sensor is integrated into the MMIC and no external LO signals need to be routed on the front end, the highest frequency of a signal connected to the MMIC is the approx. 8 GHz output of the frequency divider. This enables

using low-cost FR4 printed circuit board (PCB) material for the front end to create a low-cost THz radar sensor (similar to [22]). Furthermore, a low-cost polytetrafluoroethylene (PTFE) dielectric lens was developed to enhance the antenna directivity of the antennas on the MMIC and to shield the MMIC and bond wires from external environmental influences.

MMIC design

In this section, the separate building blocks of the fully integrated 0.48 THz FMCW radar MMIC are detailed, as elaborated in Section "System concept", and measurement results are discussed.

The radar transceiver discussed in this paper was manufactured in a development lot of the 130-nm SiGe BiCMOS technology SG13G3 from IHP (based on [32, 33]). The technology offers SiGe HBTs which a transit frequency f_T of 470 GHz, a maximum oscillation frequency f_{max} of 650 GHz, and breakdown voltages of 1.5 V BV_{CEo} and 3.7 V BV_{CBo}. The set of passive elements includes salicided and unsalicided poly-silicon resistors, metal-insulator-metal (MIM) capacitors, and MOS-based Varicaps. The metal stack consists of seven aluminum layers including five fine-structured layers and two thick top metal layers with thicknesses of 2 μm and 3 μm, respectively, for transmission lines, inductors, and transformers.

Due to compatibility issues with software packages used at the time of circuit design, no parasitic extractions could be performed on the designed circuit cores. Parasitics capacitances were estimated based on experience made in other 130 nm SiGe technologies [11, 34]. EM simulations of the designed circuit layouts were performed using Sonnet to optimize the performance of the developed circuit elements.

120 GHz VCO

A VCO is used to generate the signal on this fully integrated FMCW radar MMIC, in contrast to many other publications in the THz range, which use an external signal generation approach [17, 20]. When deciding on a center frequency (f_c) and subsequent frequency multiplication factor to generate the targeted output frequency, careful consideration has to be taken regarding the circuit architecture, tuning range, and phase noise of the oscillator. While for lower center frequencies, the phase noise, and the relative tuning range are better compared to higher frequencies, doubling the frequency results in an addition of 6 dB to the phase noise [35]. Due to the unavailability of parasitic extracted circuit simulations, a center frequency of 120 GHz was chosen, due to experience based on other 130 nm SiGe BiCMOS technologies. Furthermore, a center frequency of 120 GHz ensures a large distance of the targeted fourth harmonic at 480 GHz to other unwanted harmonics, primarily the third and fifth harmonic, at 360 and 600 GHz respectively.

The VCO of this MMIC is based on the differential Colpitts oscillator topology. A common base amplifier is used at the oscillator's output to increase the output power. It is used to drive the subsequent frequency doubler and to decouple the oscillator from influences of the following circuit stages. A voltage-controlled MOSCAP is used as the tunable circuit element of the VCO. The oscillator's output frequency can be controlled by tuning voltages between -1 and $+5$ V. The schematic diagram of the implemented VCO is depicted in Fig. 3.

As circuits in this frequency range are highly susceptible to parasitic influences, like parasitic capacitances, which in this case,
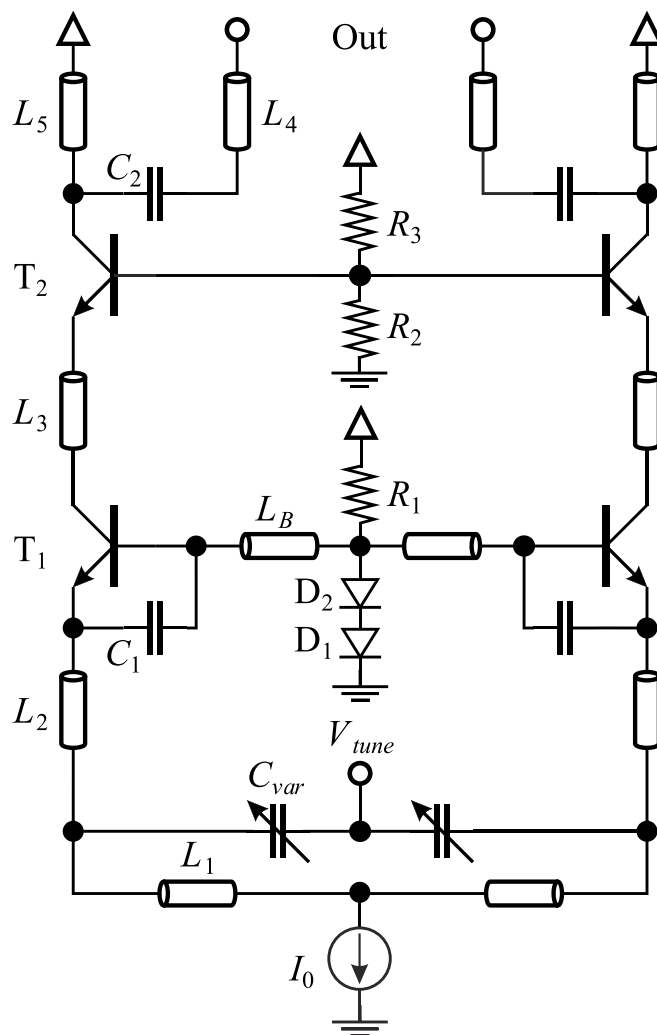

Figure 3. Schematic diagram of the implemented 120 GHz VCO. The length of the transmission line L_B can be altered with laser fuses to configure the center frequency of the oscillator.

influence the oscillator's output frequency and phase noise, laser fuses were implemented to compensate for these parasitic effects and manufacturing variances. These fuses can be removed after production to lower the center frequency f_c of the oscillator (119–108.5 GHz). The measurement results of this fully integrated signal source can be seen in Fig. 4.

The VCO, set to the highest center frequency of around 119 GHz can be tuned from 110.7 to 126.7 GHz, which leads to a tuning range (TR) of 16 GHz and relative tuning range (rTR) of 13.7%. The output power was determined to be around 7.1 dBm with a flatness of 1.2 dB while having a power consumption of only 78 mW. This leads to a dc-to-RF efficiency of up to 6.6%. The measured phase noise is between -72.5 and -82 dBc/Hz at an offset frequency Δf of 1 MHz. This phase noise measurement was performed using a Rohde & Schwarz FSWP Phase Noise Analyzer at the output of the integrated frequency divider. Due to the frequency translation of the by 16 divider, the measured phase noise was corrected by 24 dB. These measurements were performed on a dedicated breakout MMIC just containing the VCO and frequency divider (published in [36]).
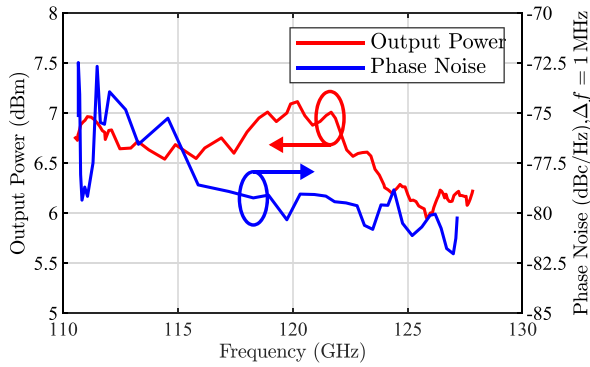
Figure 4. Measured output power and phase noise of the integrated 120 GHz VCO. No fuses were cut for this measurement. The phase noise was measured at an offset frequency Δf of 1 MHz.

Frequency divider

To stabilize the signal from the VCO with an off-chip PLL, a static by-16 frequency divider was developed. For the design of the divider, four flip-flops were utilized, which were designed in an emitter-coupled logic (ECL).

The frequency divider is directly connected to the collectors of the VCOs output amplifier and uses a buffer stage for the approx. 7.5 GHz output signal. This buffer decouples the divider from the pads and bond wires and drives off-chip loads, like PLL ICs.

We used a Keysight MSOS804A oscilloscope to measure the differential output signals of the divider. The divider generates a -10 dBm output signal over the whole tuning range of the VCO and consumes 377 mW just for the frequency divider. The operation of the frequency divider was verified up to 163 GHz using a separate breakout MMIC (published in [37]).

120–240 GHz Gilbert frequency doubler

A bootstrapped Gilbert-cell frequency doubler is used to double the frequency of the differential signal generated by the oscillator. This doubler architecture has differential input and output ports and is suitable for wideband applications [38]. A previous version of this circuit was published in [36], detailing the measurement results of a breakout MMIC, containing this frequency doubler. A schematic diagram of the implemented frequency doubler is depicted in Fig. 5.

This circuit version introduced a power splitter that splits the 240 GHz signal into the Rx and Tx path between the frequency doubler and the PAs in the respective signal paths. As we used identical power amplifiers in the Tx and Rx paths, we directly split the signal instead of implementing two Wilkinson power dividers for the differential signal.

240 GHz power amplifier

After splitting the LO signal, we use parallel PA chains for the transmit and receive paths. These PAs are implemented with a two-stage, cascaded differential cascode amplifier topology. The measurement results from a previous publication [39] show the importance of providing as much input power to the subsequent frequency doubler in the transmit path as possible. Therefore,
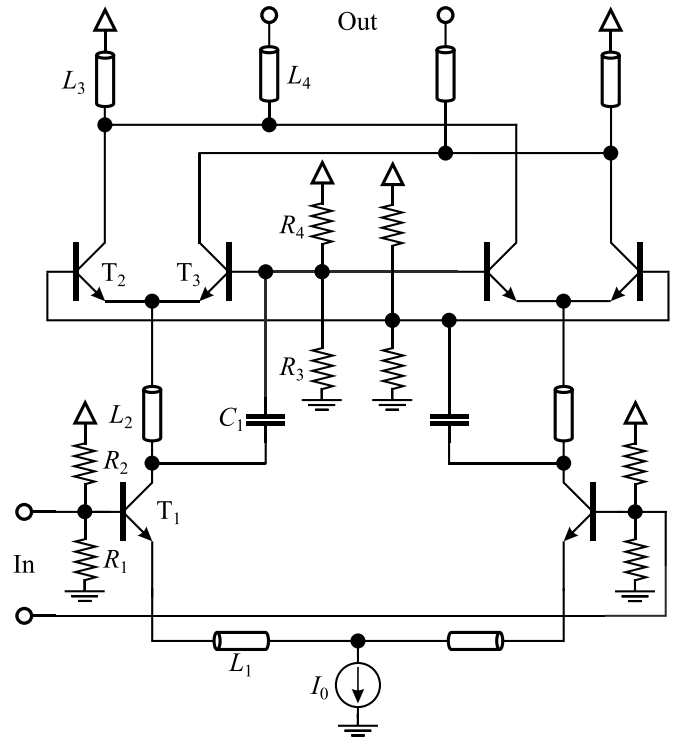

Figure 5. Schematic diagram of the developed $120 - 240$GHz frequency doubler, based on a bootstrapped Gilbert-Cell topology.

for the circuit revision on this transceiver MMIC, the matching between the PAs and the following frequency doubler in the Tx path and IQ-coupler in the Rx path was improved. The PA cores remain largely unchanged (compared to [36]), with a core current of 15.9 mA and 18.0 mA, respectively. The power amplifiers provide up to 7 dBm output power with a maximum variation of the output power of 1.6 dB over a frequency range of 35 GHz (213–248 GHz).

240–480 GHz push–push frequency doubler

The desired output frequency of 480 GHz of the radar system is almost equal to the transit frequency f_T of 470 GHz of the used transistors in the SG13G3 technology. Therefore, the second frequency doubling stage is implemented as a push-push frequency doubler, as these can reach comparatively high output powers even above the respective transit frequencies of the used transistors. Furthermore, push-push doublers achieve high fundamental suppression due to the operating principle of the frequency doubling. A downside typically brought up when using push-push doublers is the conversion from a differential input signal to a single-ended output signal. This is no drawback in this application, as a single-ended patch antenna can be used as Tx antenna. Therefore, no additional balun needs to be used to drive the antenna. A schematic diagram of the developed push–push architecture-based frequency doubler is depicted in Fig. 6.

Frequency doublers in the lower THz range often use power combining to reach even higher output powers than possible with a single doubler [40]. However, in this MMIC, we did not use power combining to keep the space and power consumption requirements low.
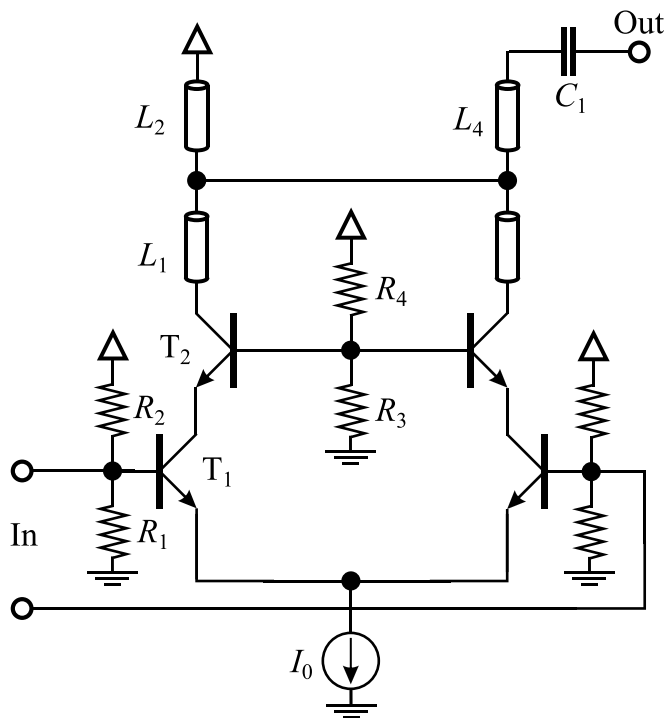
Figure 6. Schematic diagram of the implemented 240 — 480GHz push–push frequency doubler.

Figure 7. Output power measurements of the second frequency doubler for different fuse configurations of the VCO. To investigate the maximum output power of the circuit, the supply voltage was increased to 4 V for the final measurement with three fuses cut.

480 GHz subharmonic mixer

The dynamic range of the radar MMIC is mainly influenced by the transmit power of the Tx path and the receive mixer in the Rx path. Subharmonic mixer architectures are often used for THz applications, as the receive signal frequency is above the transit frequency f_T of the used technology [41–43]. Therefore, a subharmonic receive mixer architecture was implemented for this radar MMIC. A Gilbert cell with an integrated frequency doubler, utilizing quadrature LO signals, is used in this transceiver (similar to [44]). A schematic diagram of this implementation is given in Fig. 8. The quadrature LO signals are created by two microstrip branchline couplers fed by the PAs described in Section "240 GHz power amplifier".

One potential downside of this circuit architecture is the susceptibility of this circuit to amplitude or phase imbalances of the quadrature LO signals I and Q generated by the integrated microstrip branchline couplers. Although these couplers were carefully EM-simulated during the circuit design, the receiver circuit should still be investigated on its susceptibility to amplitude and phase errors. To perform this investigation, the LO signals I and Q are generated by microwave ports, and artificial phase and amplitude errors are introduced to this simulation for LO input frequencies between 200 and 250 GHz. When simulating phase errors of up to 30°, e.g., a relative phase between I and Q of 60° to 120°, a maximum degradation of the conversion gain of just 1.39 dB could be determined. By introducing an amplitude error of up to 3 dB between I and Q signals, a maximum conversion gain degradation of just 1.3 dB could be determined. These simulation results demonstrate the robustness of the developed receiver circuit against phase and amplitude imbalances. Combined with the carefully EM-simulated couplers generating the quadrature signals I and Q, this circuit architecture ensures a robust operation over the targeted frequency range.

Using the alternate characterization MMIC, already described in Section "240–480 GHz push–push frequency doubler", the operation of the receive mixer was successfully verified by feeding the MMIC with an artificial receive signal and generating the LO signals on-chip. Using a Keysight MSOS804A oscilloscope, a peak conversion gain of −16 dB was achieved at a frequency of 474 GHz [26].

Previous research and publications [39] have shown the importance of the interface between the PAs and the push-push doubler circuit. This interface and the inductive load of the doubler stage were optimized in this circuit revision to improve the output power of the doubler by more than 6 dB in relation to the previous version. This improvement was achieved, influencing neither the transistor sizes, the power consumption, nor the common-base stage of the PAs. The output power of the second frequency doubling stage was characterized on a separate radar MMIC that was just manufactured for circuit measurement and system characterization purposes. It is similar to the MMIC shown in Fig. 1, but GSG probe pads at the doubler's output and the mixer's input are placed instead of the patch antennas.

Using this MMIC, an output power of up to −12.6 dBm with a supply voltage of 3.3 V and up to −9.4 dBm with a supply voltage of 4 V was measured for this circuit. The measurement results of the 240 to 480 GHz frequency doubler for different fuse configurations of the VCO core are depicted in Fig. 7. The output power of the circuit is measured using an Erickson PM5B power meter with a corresponding Formfactor T-Wave Probe and a WR2.2 to WR10 rectangular waveguide taper. The losses of the probe, taper, and GSG pad are de-embedded from the measured output power using measurement data of these elements.

It can be seen that the performance of the 240–480 GHz frequency doubler is mainly limited by the tuning range of the VCO. Below a frequency of 470 GHz, the output power of the doubler is mainly flat, with only a minor difference between the individual measurement curves. The difference between the curves can be explained by the fact that the MMIC has to be removed from the wafer-prober to cut the fuses and re-contacted with the probes for the subsequent measurement. Slight variations in the probes' positioning and in contact resistance lead to minor differences in the measurement curves.
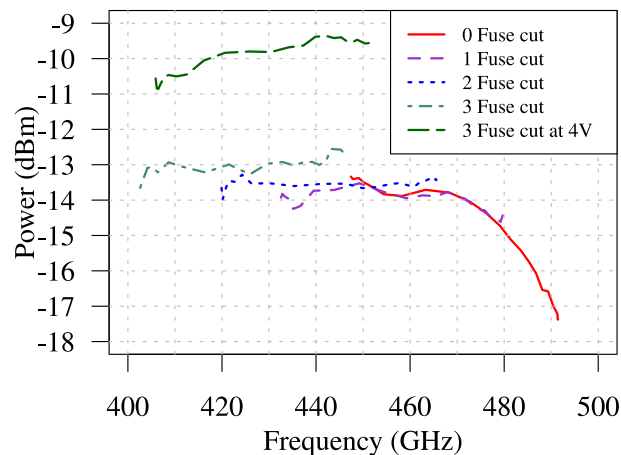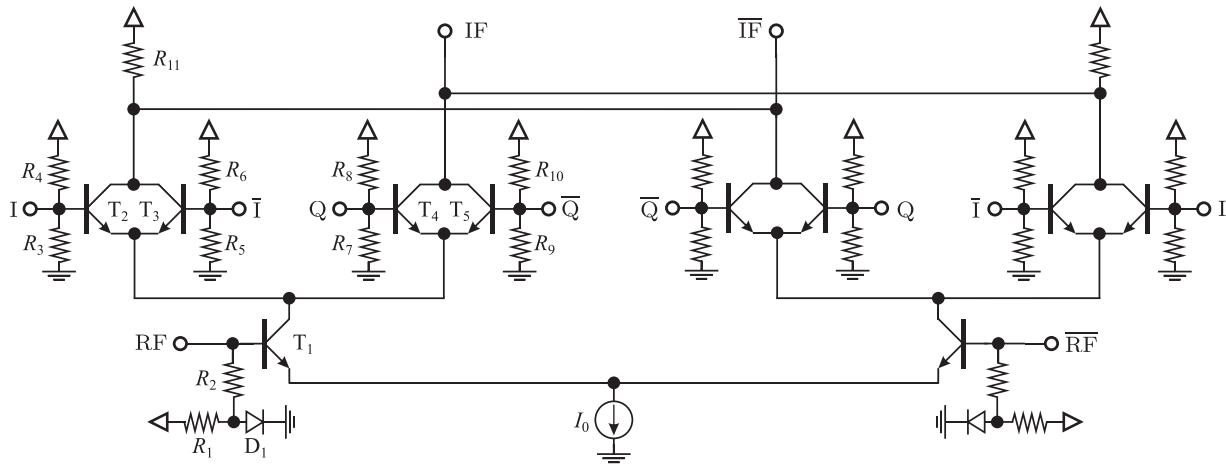
Figure 8. Schematic diagram of the implemented subharmonic 480 GHz receive mixer. The LO input signals I, Ī, Q, and Q̄ are generated by two microstrip branchline couplers.
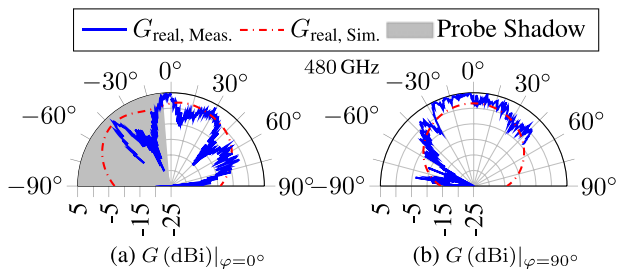

Figure 9. Realized gain at 480 GHz: (a) $\vec{E}$- and (b) $\vec{H}$-plane of the Tx patch antenna.

On-chip 480 GHz antennas

To transmit and receive the radar signals, the push–push frequency doubler and subharmonic mixer are connected to two patch antennas integrated on the MMIC. The antennas are designed for a center frequency f_c of 480 GHz and have a length of around 150 μm. To improve the matching of the antennas, inset feeding is implemented in both the single-ended transmit antenna Tx and the differential receive antenna Rx.

For characterization purposes, the Tx antenna was manufactured on a breakout MMIC with GSG probe pads and was measured with the setup from [45].

In Fig. 9, the measurement results for the antenna at a frequency of 480 GHz are shown as $\vec{E}$- and $\vec{H}$-plane cuts. A maximum gain of 3 dBi was measured at a frequency of 460 GHz. Overall the measurements show a good agreement compared to the full-wave FDTD simulation results.

It should be noted that, due to the high frequency, reflections from the probe contribute to the measured radiation pattern yielding the undulations on the measured patterns [46]. Furthermore, a part of the measured radiation pattern is shadowed by the probe. Hence, the measurement results cannot be interpreted here [47]. The Rx antenna is not characterized, as it is highly similar to Tx, and would, however, require a balun and more breakout-chip area for separate measurement.

Dielectric lens antenna

To improve the measurement range and focus the radar beam in one direction, a dielectric lens, based on the work in [34, 48, 49],
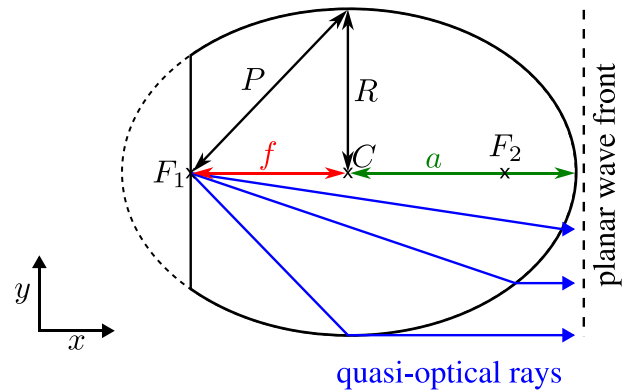

Figure 10. Cross-section of the lens concept.

was developed to enhance the antenna gain described in Section "On-chip 480 GHz antennas". In addition to improving the antenna gain, the dielectric lens has the supplementary benefit of shielding the radar MMIC against outside influences and protecting the fragile wire bonds, connecting the MMIC to the FR4 frontend PCB.

The dielectric lens is based on a rotationally symmetrical elliptical lens manufactured from PTFE. This material was chosen for its low dielectric loss tangent $tan \, \delta \approx 0.0004$, dielectric constant $\epsilon_r = 2.08$, and good machining properties [34, 48, 49]. The shape of the elliptic lens is given by a modification of the standard ellipse equation:

$$1 = \left(\frac{x}{a}\right)^2 + \left(\frac{y}{R}\right)^2. \tag{1}$$

When the feeding of the lens is done at the focal point F_1 of the lens, which is located at a distance f from the center C of the ellipse, and the quasi-optic rays are refracted parallel to the rotation axis in the boresight direction of x [50], the distance f can be calculated depending on the radius of the lens R and the dielectric constant ϵ_r of the lens material (cf. (2)). The cross-section of this concept can be seen in Fig. 10.

$$f = R \cdot \tan\left(\sin^{-1}\left(\frac{1}{\sqrt{\epsilon_r}}\right)\right) = R \cdot \frac{1}{\sqrt{\epsilon_r - 1}}. \tag{2}$$

The second semi-axis a of the lens can also be calculated depending on the radius R and the dielectric constant ϵ_r, as the quasi-optic rays have to form a plane phase front at the tip of the lens. This means that the following equation has to be true:

$$\frac{\sqrt{\epsilon_r}}{c_0} \cdot (f + a) = P \cdot \frac{\sqrt{\epsilon_r}}{c_0} + a \cdot \frac{1}{c_0}. \tag{3}$$

By rearranging (3), the length of the second semi-axis a can be calculated:

$$a = R \cdot \frac{\sqrt{\epsilon_r}}{\sqrt{\epsilon_r - 1}} = R \cdot \frac{1}{\sqrt{1 - \frac{1}{\epsilon_r}}}. \tag{4}$$

Substituting the results from (2) and (4) into (1) and defining the feeding point of the lens at the focal point F_1, the shape of the dielectric lens can be described in dependence of the radius R and the dielectric constant ϵ_r of the lens:

$$1 = \left(\frac{x - f}{a}\right)^2 + \left(\frac{y}{R}\right)^2, \tag{5}$$

$$= \left(\frac{x - \frac{R}{\sqrt{1 - 1/\epsilon_r}}}{\frac{R}{\sqrt{1 - 1/\epsilon_r}}}\right)^2 + \left(\frac{y}{R}\right)^2. \tag{6}$$

The radius R of the lens can be chosen depending on the targeted application, antenna gain, and form factor of the radar system. To estimate the directivity D of the dielectric lens, the following estimation was used [51]:

$$D = \frac{4 \cdot \pi \cdot A_E}{\lambda^2}. \tag{7}$$

In this equation, the losses of the dielectric lens antenna are neglected. Using the approximation of $A_E \approx \pi \cdot R^2$, a maximum theoretical directivity of 45 dBi can be calculated for a dielectric lens with a radius $R = 18$ mm using Eq. (7). A radius of $R = 18$ mm was chosen because of the aspect that a small and lightweight THz radar system is going to be implemented with this lens. Hence, this radius is a good tradeoff between the small form factor and the targeted measurement range of the radar system.

To verify this approximation, a simulation model was implemented in CST Microwave Studio. There is a large discrepancy between the feature size of the on-chip antennas, which have a minimum feature size of 420 nm, and the dielectric lens, which has a radius R of 18 mm. Because of this discrepancy, a simulation of the on-chip antennas in combination with the dielectric lens would take vast amounts of time and simulation power. Therefore, a two-stage approach was chosen for this simulation to assess the performance of the patch antennas in conjunction with the lens.

As a first step, the on-chip patch antennas were simulated, and near-field sources of both antennas were created. These near-field sources were included in the simulation environment of the dielectric lens. In this simulation environment, the physical construction of the MMIC in an open QFN package inside a cavity of the lens is modeled, as depicted in Fig. 11. The dielectric lens and QFN package are mounted on an FR4 PCB with a grounded metal plane as the top layer. Including the mounting interface to attach the lens to the PCB, the lens has a height of 43.3 mm.
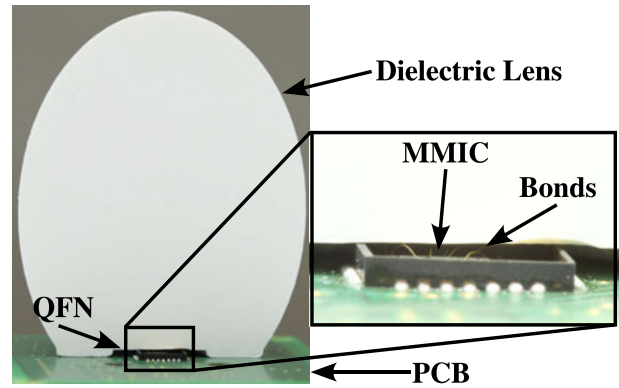

Figure 11. Cross-section of the presented assembly. The dielectric lens is visualized by a non-functional 3D-printed cut model.

The simulation results of the transmit and receive path in the $\vec{E}$- and $\vec{H}$-plane using this model and the detailed two-step simulation approach can be seen in Fig. 12(a) and 12(b).

It can be seen that both paths of the radar system, transmit path (Tx) as well as receive path (Rx), have a distinctive peak of the directivity of around 41.7 dBi with a half-power beam width (HPBW) of 1.5°. Because of the bistatic approach, the on-chip antennas cannot be placed in the symmetry plane of the dielectric lens in the $\vec{E}$-plane but are shifted 175 μm to either side of the symmetry plane. This shift leads to two squinting beams with a beam direction of 0.5° in either direction.

As the presented transceiver has a separate transmit and receive path with corresponding integrated antennas, it has to be handled as a bistatic radar sensor. The radar range equation for a bistatic radar system is given by:

$$P_{Rx} = P_{Tx} \frac{D_{Tx} D_{Rx} \lambda^2 \sigma}{(4\pi)^3 R_{Tx}^2 R_{Rx}^2}. \tag{8}$$

In this equation, the power at the receiver P_{Rx} is dependent on the power from the transmitter P_{Tx}, the directivities of the receive (D_{Rx}) and transmit (D_{Tx}) antenna, the wavelength λ of the radar signal, the radar cross-section σ of the target, and the distances between the transmitter and receiver to the target, described by the factors R_{Tx} and R_{Rx}. Due to the small pitch between transmit and receive antenna, the distances R_{Tx} and R_{Rx} are practically identical. Therefore the term $R_{Tx}^2 R_{Rx}^2$ in Eq. 8 can be replaced by R^4. The system can also be handled as a monostatic radar transceiver because of the small distance between the transmitter and receiver and the similar transmit and receive characteristics. The term $D_{Tx} D_{Rx}$ can be replaced by D_{eff}^2, where D_{eff} describes the effective directivity of the radar system. This simplifies Eq. 8 to the following equation for a monostatic radar system:

$$P_{Rx} = P_{Tx} \frac{D_{eff}^2 \lambda^2 \sigma}{(4\pi)^3 R^4}. \tag{9}$$

This effective directivity represents the bistatic squinting assembly, with a monostatic model calculated by combining the directivities in transmit and receive operation. It can be determined by calculating the geometric mean of the Tx and Rx directivity for every angle θ and φ:

$$D_{eff}(\theta, \varphi) = \sqrt{D_{Tx}(\theta, \varphi) \cdot D_{Rx}(\theta, \varphi)}. \tag{10}$$

(a) Directivity: $\vec{E}$-plane
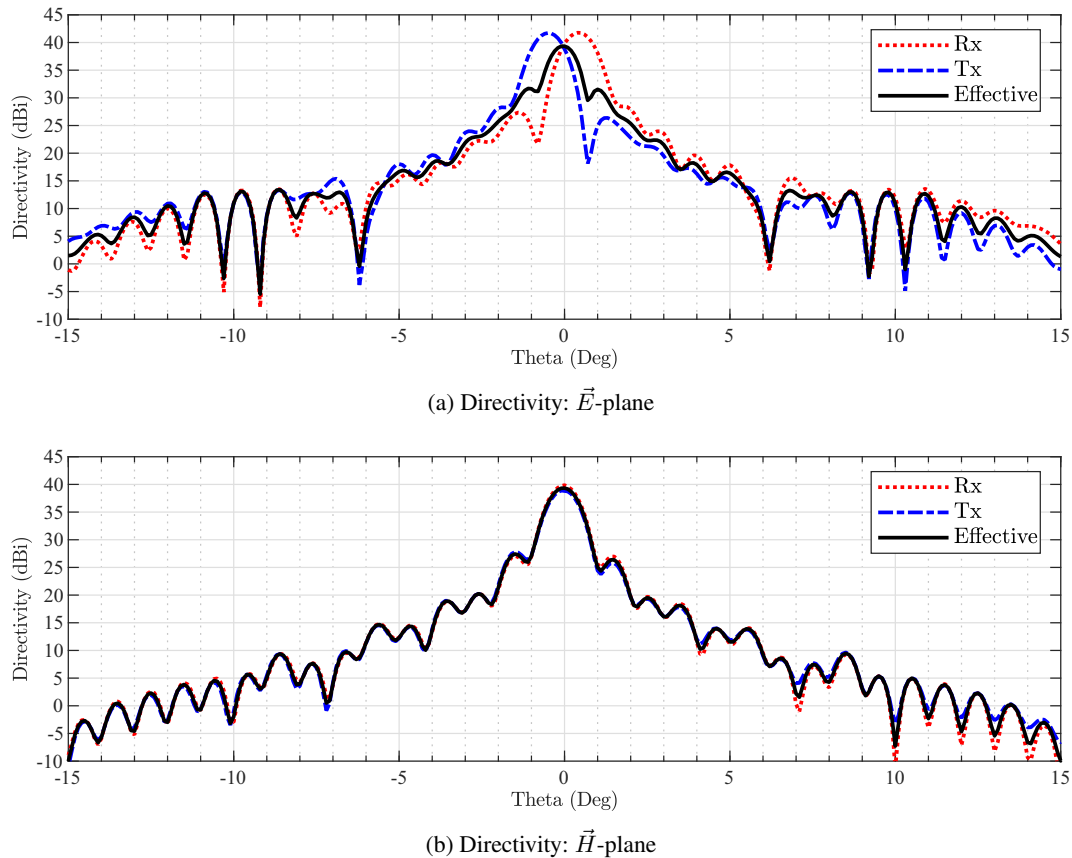

(b) Directivity: $\vec{H}$-plane

Figure 12. Simulation results of the proposed MMIC and dielectric lens combination in the $\vec{E}$ and $\vec{H}$-plane. Squinting beams for the Rx and Tx path can be observed in the $\vec{E}$-plane, but not in the $\vec{H}$-plane. No squinting can be observed for the resulting effective beams in $\vec{E}$ or $\vec{H}$-plane. (a) Directivity: $\vec{E}$-plane. (b) Directivity: $\vec{H}$-plane.

The effective directivity, calculated by the equation above (10), is depicted in black in Fig. 12(a) and 12(b). The effective directivity has its peak in the boresight direction and is approximately 2.4 dB lower than the respective Tx and Rx beams in the $\vec{E}$-plane. Due to the small pitch of the antennas of only 350 μm, the geometric mean of both individual beams leads to a distinctive peak of 39.33 dBi in the $\vec{E}$-plane. Because of the combination of the two squinting beams, the sidelobe level in the $\vec{E}$-plane is considerably higher than the respective individual Tx and Rx beams, with a value of 7.64 dB. The HPBW of the effective directivity in the $\vec{E}$-plane is 0.95°. As the on-chip antennas lie on the symmetry plane for the directivity in the $\vec{H}$-plane, no squinting of the Rx and Tx beams can be observed in Fig. 12(b). The effective directivity in the $\vec{H}$-plane reaches a value of 39.3 dBi in boresight direction with an HPBW of 0.95° and a sidelobe level of 11.91 dB.

The simulation results show that this dielectric lens enables a compact and low-cost 0.48 THz FMCW radar system with a small beam width and high suppression of unwanted targets for high-accuracy measurement scenarios.

Comparison to state-of-the-art electronic THz transceivers

In Table 1, the proposed 0.48 THz transceiver is compared to the state of the art in electronic THz transceivers. The comparison of the size and power consumption P_{dc} has to be split between systems with external signal generation, typically using a laboratory signal generator, and the transceivers that generate the signal

internally with integrated VCOs. As in the realization described in this manuscript, most comparable THz transceivers use lenses to improve the radiation characteristics of the antennas integrated on their respective transceiver MMICs. These lenses are manufactured from multiple different materials, like polymethylpentene (TPX), polypropylene (PP), silicon (Si), or in this case, made from PTFE.

Conclusion

This paper shows a fully integrated transceiver operating in the range of 0.448–0.491 THz. Besides the transmit and receive path, the frequency divider is also integrated on the MMIC. This makes it possible to use an external PLL IC to create a complete radar system. The receiver channel features a subharmonic down-conversion mixer that enables the use of 240 GHz quadrature signals and a differential patch antenna. The transmit signal is generated with a push-push frequency doubler and a single-ended patch antenna, reaching −9.4 dBm. This radar MMIC is complemented by a dielectric lens design to improve the directivity of the integrated patch antennas. The dielectric lens reaches directivities of up to 39.3 dBi in boresight direction and narrows the beam to a HPBW of just 0.95°, improving the measurement range of the radar system. Furthermore, it provides a high suppression of more than 24.6 dB for clutter from unwanted targets, deviating more than 6° from antenna boresight in the $\vec{E}$- and $\vec{H}$-plane. In summary, the transceiver presented is the first to be fully integrated and to have an output frequency just below 0.5 THz.

Table 1. Comparison of state-of-the-art integrated electronic THz transceivers

Ref.	Technology	Signal generation	f_c (GHz)	TR (GHz)	P_{Out} (dBm)	P_{dc} (mW)	Antenna concept	Size* (mm²)
[30]	65 nm CMOS	Ext. 14 GHz LO	270	100	−1.5	840	SIW dual-slot ant. + TPX lens	5
[27]	130 nm SiGe	Ext. 18 GHz LO	320	43	−5	2944	Tx: Slot ant. + Si lens Rx: Folded dipole ant. + Si lens	1.98
[16]	130 nm SiGe	Integr. 160 GHz VCO	321	38.43	3	722	Tx: Return path gap radiator + Si lens Rx: Patch ant. + Si lens	5.14
[15]	130 nm SiGe	Integr. 85 GHz VCO	340	52	−6.8	640	Patch ant.	1.2
[12]	130 nm SiGe	Integr. 170 GHz VCO	340	70	0.1	1700	Patch ant. + TPX lens	2.85
[14]	130 nm SiGe	Integr. 93 GHz VCO	380	14.6	−11**	380	Patch ant.	4.18
[20]	35 nm & 50 nm InAlAs/InGaAs	Ext. 8 GHz LO	383	80	9	1100	Patch ant. with dielectric resonator and metastructured GND plane + PP lens	9
[13]	40 nm CMOS	Ext. 17.5 GHz LO	420	CW	−9	905	Folded dipole ant. + Si lens	4.88
[17]	90 nm SiGe	Ext. 20 GHz LO	470	55	−10	280	Patch ant. with parasitic patches	1.42
This work	130 nm SiGe	Integr. 120 GHz VCO	480	43	-12.6	877	Patch ant. + PTFE lens	1.92

*Size of all MMICs that form the transceiver.
**EIRP.

References

1. Hillger P, van Delden M, Thanthrige USM, Ahmed AM, Wittemeier J, Arzi K, Andree M, Sievert B, Prost W, Rennings A, Erni D, Musch T, Weimann N, Sezgin A, Pohl N and Pfeiffer UR (2020) Toward mobile integrated electronic systems at THz frequencies. *Journal of Infrared Millimeter and Terahertz Waves* **41**(7), 846–869.
2. Kissinger D, Kahmen G and Weigel R (2021) Millimeter-wave and terahertz transceivers in SiGe BiCMOS technologies. *IEEE Transactions on Microwave Theory and Techniques* **69**(10), 4541–4560.
3. Kissinger D (2022) Integrated circuits in SiGe BiCMOS for millimeter-wave and terahertz bioanalyzers. In *2022 IEEE MTT-S Int. Microw. Workshop Ser. Adv. Mater. Process. RF THz Appl. (IMWS-AMP)*. IEEE, Guangzhou, China, pp. 1–3.
4. Abouzaid S, Jaeschke T, Barowski J and Pohl N (2022) FMCW radar-based material characterization using convolutional neural network and K-means clustering. In *2022 24th Int. Microw. Radar Con. (MIKON)*. IEEE, Gdansk, Poland, pp. 1–4.
5. Kueppers S, Jaeschke T, Pohl N and Barowski J (2022) Versatile 126–182 GHz UWB D-band FMCW radar for industrial and scientific applications. *IEEE Sensors Letters* **6**(1), 14–17.
6. Barowski J and Rolfes I (2017) Millimeter wave material characterization using FMCW-transceivers. In *2017 IEEE MTT-S Int. Microw. Workshop Ser. Adv. Mater. Processes RF THz Appl. (IMWS-AMP)*. IEEE, Pavia, Italy, pp. 1–3.
7. Wittemeier J, Ahmed AM, Tran TN, Sezgin A and Pohl N (2020) 3D localization using a scalable FMCW MIMO radar design. In *2020 German Microw. Conf. (GeMiC)*. IEEE, Cottbus, Germany, pp. 100–103.
8. Krems T, Haydl W, Massler H and Rudiger J (1996) Millimeter-wave performance of chip interconnections using wire bonding and flip chip. In *1996 IEEE MTT-S Int. Microw. Symp. Dig.* IEEE, San Francisco, CA, pp. 247–250.
9. Wang Y, Yi X, Xu J, Zheng B, Che W and Xue Q (2022) Gain enhancement of millimeter-wave on-chip antenna through low-cost packaging technology. In *2022 IEEE 10th Asia-Pacific Conf. Antennas Propag. (APCAP)*. IEEE, Xiamen, China, pp. 1–2.
10. Ahmed F, Furqan M, Aufinger K and Stelzer A (2021) A 240-GHz FMCW radar transceiver with 10 dBm output power using quadrature combining. In *2020 15th Eur. Microw. Integr. Circuits Conf. (EuMIC)*. IEEE, Utrecht, Netherlands, pp. 281–284.
11. Bredendiek C, Pohl N, Jaeschke T, Aufinger K and Bilgic A (2013) A 240 GHz single-chip radar transceiver in a SiGe bipolar technology with on-chip antennas and ultra-wide tuning range. In *2013 IEEE Radio Freq. Integr. Circuits Symp. (RFIC)*. IEEE, Seattle, WA, USA, pp. 309–312.
12. Al-Eryani J, Knapp H, Kammerer J, Aufinger K, Li H and Maurer L (2018) Fully integrated single-chip 305–375-GHz transceiver with on-chip antennas in SiGe BiCMOS. *IEEE Transactions on Terahertz Science and Technology* **8**(3), 329–339.
13. Simic D, Guo K and Reynaert P (2021) A 420-GHz sub-5-μm range resolution TX-RX phase imaging system in 40-nm CMOS technology. *IEEE Journal of Solid-State Circuits* **56**(12), 3827–3839.
14. Park J-D, Kang S and Niknejad AM (2012) A 0.38 THz fully integrated transceiver utilizing a quadrature push-push harmonic circuitry in SiGe BiCMOS. *IEEE Journal of Solid-State Circuits* **47**(10), 2344–2354.
15. Jalili H and Momeni O (2019) A 0.34-THz wideband wide-angle 2-D steering phased array in 0.13-μm SiGe BiCMOS. *IEEE Journal of Solid-State Circuits* **54**(9), 2449–2461.
16. Jiang C, Mostajeran A, Han R, Emadi M, Sherry H, Cathelin A and Afshari E (2016) A fully integrated 320 GHz coherent imaging transceiver in 130 nm SiGe BiCMOS. *IEEE Journal of Solid-State Circuits* **51**(11), 2596–2609.
17. Mangiavillano C, Kaineder A, Aufinger K and Stelzer A (2022) A 1.42-mm² 0.45–0.49 THz monostatic FMCW radar transceiver in 90-nm SiGe BiCMOS. *IEEE Transactions on Terahertz Science and Technology* **12**(6), 592–602.

18. **Caris M, Stanko S, Palm S, Sommer R, Wahlen A and Pohl N** (2015) 300 GHz radar for high resolution SAR and ISAR applications. In *2015 16th Int. Radar Symp. (IRS)*. IEEE, Dresden, Germany, pp. 577–580.

19. **Gashi B, John L, Meier D, Rösch M, Wagner S, Tessmann A, Leuther A, Ambacher O and Quay R** (2021) Broadband 400-GHz InGaAs mHEMT transmitter and receiver S-MMICs. *IEEE Transactions on Terahertz Science and Technology* **11**(6), 660–675.

20. **Baumann B, Gashi B, Meier D and Zech C** (2022) High-resolution 400 GHz submillimeter-wave quasi-optical radar imaging system. *IEEE Microwave and Wireless Components Letters* **32**(3), 226–229.

21. **Hillger P, Grzyb J, Jain R and Pfeiffer UR** (2019) Terahertz imaging and sensing applications with silicon-based technologies. *IEEE Transactions on Terahertz Science and Technology* **9**(1), 1–19.

22. **Thomas S, Bredendiek C and Pohl N** (2019) A SiGe-based 240-GHz FMCW radar system for high-resolution measurements. *IEEE Transactions on Microwave Theory and Techniques* **67**(11), 4599–4609.

23. **Geiger M, Gut S, Hügler P and Waldschmidt C** (2020) Flexible radar front end with multimodal transition at 300 GHz. In *2020 IEEE/MTT-S Int. Microw. Symp. (IMS)*. IEEE, Los Angeles, CA, pp. 639–642.

24. **Setiawan A, Yamawaki A, Yonemoto N, Nohmi H and Murata H** (2022) Millimeter-wave imaging using dielectric lens for security application. In *2022 19th Eur. Radar Conf. (EuRAD)*. IEEE, Milan, Italy, pp. 225–228.

25. **Muckermann N, Barowski J and Pohl N** (2022) A large distance focus dielectric Fresnel-based lens antenna for millimeter wave radar. In *2022 52nd Eur. Microw. Conf. (EuMC)*. IEEE, Milan, Italy, pp. 608–611.

26. **Starke D, Wittemeier J, Vogelsang F, Sievert B, Erni D, Rennings A, Rucker H and Pohl N** (2022) A fully integrated 0.48 THz FMCW radar transceiver MMIC in a SiGe-technology. In *2022 17th Eur. Microw. Integr. Circuits Conf. (EuMIC)*. IEEE, Milan, Italy, pp. 56–59.

27. **Statnikov K, Öjefors E, Grzyb J, Chevalier P and Pfeiffer UR** (2013) A 0.32 THz FMCW radar system based on low-cost lens-integrated SiGe HBT front-ends. In *2013 Proc. ESSCIRC (ESSCIRC)*. IEEE, Bucharest, Romania, pp. 81–84.

28. **Grzyb J, Statnikov K, Sarmah N, Heinemann B and Pfeiffer UR** (2016) A 210–270-GHz circularly polarized FMCW radar with a single-lens-coupled SiGe HBT chip. *IEEE Transactions on Terahertz Science and Technology* **6**(6), 771–783.

29. **Merkle T, Meier D, Wagner S, Tessmann A, Kuri M, Massler H and Leuther A** (2019) Broadband 240-GHz radar for non-destructive testing of composite materials. *IEEE Journal of Solid-State Circuits* **54**(9), 2388–2401.

30. **Yi X, Wang C, Chen X, Wang J, Grajal J and Han R** (2021) A 220-to-320-GHz FMCW radar in 65-nm CMOS using a frequency-comb architecture. *IEEE Journal of Solid-State Circuits* **56**(2), 327–339.

31. Direct Modulation/Fast Waveform Generating, 13 GHz, Fractional-N Frequency Synthesizer, Analog Devices. (2014) rev. E. [Online]. https://www.analog.com/media/en/technical-documentation/data-sheets/ADF4159.pdf.

32. **Heinemann B, Rücker H, Barth R, Bärwolf F, Drews J, Fischer GG, Fox A, Fursenko O, Grabolla T, Herzel F, Katzer J, Korn J, Krüger A, Kulse P, Lenke T, Lisker M, Marschmeyer S, Scheit A, Schmidt D, Schmidt J, Schubert MA, Trusch A, Wipf C and Wolansky D** (2016) SiGe HBT with f_t/f_{max} of 505 GHz/720 GHz. In *2016 IEEE Int. Electron Devices Meeting (IEDM)*. IEEE, San Francisco, CA, 3.1.1–3.1.4.

33. **Rücker H and Heinemann B** (2019) Device architectures for high-speed SiGe HBTs. In *2019 IEEE BiCMOS Compound Semicond. Integr. Circuits Technol. Symp. (BCICTS)*. IEEE, Nashville, TN, pp. 1–7.

34. **Thomas S, Bredendiek C, Jaeschke T, Vogelsang F and Pohl N** (2016) A compact, energy-efficient 240 GHz FMCW radar sensor with high modulation bandwidth. In *2016 German Microw. Conf. (GeMiC)*. IEEE, Bochum, Germany, pp. 397–400.

35. **Siddiq K, Hobden MK, Pennock SR and Watson RJ** (2019) Phase noise in FMCW radar systems. *IEEE Transactions on Aerospace and Electronic Systems* **55**(1), 70–81.

36. **Vogelsang F, Starke D, Wittemeier J, Rücker H and Pohl N** (2020) A highly-efficient 120 GHz and 240 GHz signal source in a SiGe-technology. In *2020 IEEE BiCMOS Compound Semicond. Integr. Circuits Technol. Symp. (BCICTS)*. IEEE, Monterey, CA, pp. 1–4.

37. **Vogelsang F, Bredendiek C, Schöpfel J, Rücker H and Pohl N** (2022) A static frequency divider up to 163 GHz in SiGe-BiCMOS technology. In *2022 IEEE BiCMOS Compound Semicond. Integr. Circuits Technol. Symp. (BCICTS)*. IEEE, Phoenix, AZ, pp. 49–52.

38. **Kueppers S, Aufinger K and Pohl N** (2017) A fully differential 100–140 GHz frequency quadrupler in a 130 nm SiGe:C technology for MIMO radar applications using the bootstrapped Gilbert-cell doubler topology. In *2017 IEEE 17th Topical Meeting Silicon Monolithic Integr. Circuits RF Syst. (SiRF)*. IEEE, Phoenix, AZ, pp. 37–39.

39. **Wittemeier J, Vogelsang F, Starke D, Rücker H and Pohl N** (2021) A SiGe based 0.48 THz signal source with 45 GHz tuning range. In *2021 16th Eur. Microw. Integr. Circuits Conf. (EuMIC)*. IEEE, London, UK, pp. 869–872.

40. **Güner A, Mausolf T, Wessel J, Kissinger D and Schmalz K** (2021) A 440–540-GHz transmitter in 130-nm SiGe BiCMOS. *IEEE Microwave and Wireless Components Letters* **31**(6), 779–782.

41. **Deng J, Lu Q, Jia D, Yang Y and Zhu Z** (2018) Wideband fourth-harmonic mixer operated at 325–500 GHz. *IEEE Microwave and Wireless Components Letters* **28**(3), 242–244.

42. **Güner A, Mausolf T, Wessel J, Kissinger D and Schmalz K** (2020) A 440–540-GHz subharmonic mixer in 130-nm SiGe BiCMOS. *IEEE Microwave and Wireless Components Letters* **30**(12), 1161–1164.

43. **Zhou J and Luo X** (2021) An 820-GHz down-converter with fourth subharmonic mixer in 40-nm CMOS technology. *IEEE Microwave and Wireless Components Letters* **31**(10), 1146–1149.

44. **Kodkani RM and Larson LE** (2007) An integrated 50-GHz SiGe sub-harmonic mixer/downconverter with a quadrature ring VCO. In *2007 Topical Meeting Silicon Monolithic Integr. Circuits RF Syst.* IEEE, Long Beach, CA, pp. 223–226.

45. **Sievert B, Svejda JT, Erni D and Rennings A** (2020) Spherical mm-Wave/THz antenna measurement system. *IEEE Access* **8**, 89 680–89 691.

46. **Boehm L, Hitzler M, Roos F and Waldschmidt C** (2016) Probe influence on integrated antenna measurements at frequencies above 100 GHz. In *2016 46th Eur. Microw. Con. (EuMC)*. IEEE, London, UK, pp. 552–555.

47. **Titz D, Ferrero F and Luxey C** (2012) Development of a millimeter-wave measurement setup and dedicated techniques to characterize the matching and radiation performance of probe-fed antennas. *IEEE Antennas and Propagation Magazine* **54**(4), 188–203.

48. **Pohl N** (2010) A dielectric lens antenna with enhanced aperture efficiency for industrial radar applications. In *IEEE Middle East Conf. Antennas Propag. (MECAP 2010)*. Cairo, Egypt, pp. 1–5.

49. **Pohl N and Gerding M** (2012) A dielectric lens-based antenna concept for high-precision industrial radar measurements at 24 GHz. In *2012 42nd Eur. Microw. Conf. (EuMC)*. IEEE, Amsterdam, Netherlands, pp. 731–734.

50. **Olver A and Saleeb A** (1983) Improved radiation characteristics of conical horns with plastics-foam lenses. *IEE Proceedings H (Microwaves, Optics and Antennas)* **130**(3), 197–202.

51. **Stutzman W** (1998) Estimating directivity and gain of antennas. *IEEE Antennas and Propagation Magazine* **40**(4), 7–11.

David Starke was born in Herne, Germany, in 1992. He received the B.Sc. and M.Sc. degrees in electrical engineering and information technology from Ruhr University Bochum, Bochum, Germany in 2015 and 2017, respectively. Since 2017, he has been a Research Assistant with the Institute of Integrated Systems, Ruhr University Bochum, Bochum, Germany. His current research interests include mm-wave to THz radars and monolithic microwave integrated circuit (MMIC) design using silicon-germanium technologies.

Jonathan Bott (formerly Wittemeier) was born in Lünen, Germany. He received the B.Sc. and M.Sc. degrees in electrical engineering and information technology from TU Dortmund University, Dortmund, Germany, in 2014 and 2016, respectively. Between 2016 and 2017, he worked in the automotive industry as a Software Developer. Since 2017, he has been a Research Assistant at the Institute of Integrated Systems, Ruhr University Bochum. His research interests include mm-wave radar system design, circuit and MMIC design using Silicon-Germanium, as well as MIMO DoA and imaging algorithms.

Florian Vogelsang was born in Hattingen, Germany in 1993. He received the B.Sc and M.Sc. degrees in electrical engineering and information technology from Ruhr University Bochum, Bochum, Germany in 2015 and 2017, respectively. Since 2018, he has been a Research Assistant with the Institute of Integrated Systems, Ruhr University Bochum, Bochum, Germany. His current research interests include wideband radar systems in the mm-Wave and THz range, realized as monolithic microwave integrated circuits (MMIC) in silicon-germanium technologies.

Benedikt Sievert was born in Krefeld, Germany. He received his B.Sc. and M.Sc. in Electrical Engineering/High-Frequency Systems from the University of Duisburg-Essen in 2017 and 2019, respectively. Since 2017 he is a member of the Laboratory of General and Theoretical Electrical Engineering of the University of Duisburg-Essen. His research interests include mm-wave on-chip antennas, electromagnetic metamaterials, theoretical and computational electromagnetics.

Jan Barowski was born in Bochum, Germany, in 1988. He received the B.Sc. and M.Sc. degrees in electrical engineering and the Dr.Ing. degree (with honors) in electrical engineering from Ruhr University Bochum, Bochum, Germany, in 2010, 2012, and 2017, respectively. Since 2012, he has been with the Institute of Microwave Systems, headed by Ilona Rolfes, Ruhr University Bochum, as a Research Assistant. He is currently a Postdoctoral Research Scientist with the Institute of Microwave Systems. His research interests include radar signal processing, radar imaging, and material characterization techniques. Dr. Barowski was the recipient of the IEEE Antennas and Propagation Society Doctoral Research Grant in 2016 and the IEEE MTT IWMS-AMP Best Student Paper Award in 2017, U.R.S.I. Germany Sections Young Scientist Award and the German Association for Electrical, Electronic and Information Technologies (VDE) Award for the Doctoral dissertation, in 2018.

Christian Schulz received the Dipl.Ing. and Dr.Ing. degrees in electrical engineering from Ruhr University Bochum, Bochum, Germany, in 2009 and 2016, respectively. From 2010 to 2016, he was a Research Assistant with the Institute of Microwave Systems, Ruhr University Bochum, where he has been a Postdoctoral Researcher since 2016. His research interests include 3-D electromagnetic field simulations, plasma diagnostics, radar systems, and antenna design. Dr. Schulz was the recipient of the IEEE Antennas and Propagation Society Doctoral Research Award in 2014, the IEEE Microwave Theory and Techniques Society (IEEE MTT-S) Graduate Fellowship Award in 2015, and the Gert Massenberg Award for Doctoral dissertation in 2017.

Holger Rücker received his diploma and doctorate in physics from the Humboldt University of Berlin, Germany, in 1986 and 1988, respectively. From 1989 to 1991, he was a staff member of the Humboldt University of Berlin. From 1991 to 1992, he was with the Max Planck Institute for Solid State Research in Stuttgart, Germany. He joined IHP in Frankfurt (Oder), Germany in 1992 where he is engaged in research on the physics and fabrication of semiconductor devices. His research interests include SiGe bipolar devices, the development of CMOS and BiCMOS technologies, and their application in radio-frequency integrated circuits. He led the development of IHP's 130-nm SiGe BiCMOS technologies SG13S, SG13G2, and SG13G3.

Andreas Rennings studied electrical engineering at the University of Duisburg-Essen, Germany. He carried out his diploma work during a stay at the University of California in Los Angeles. He received his Dipl.-Ing. and Dr.-Ing. degrees from the University of Duisburg-Essen in 2000 and 2008, respectively. From 2006 to 2008 he was with IMST GmbH in Kamp-Lintfort, Germany, where he worked as an RF engineer. Since then, he is a senior scientist and principal investigator at the Laboratory for General and Theoretical Electrical Engineering of the University of Duisburg-Essen. His general research interests include all aspects of theoretical and applied electromagnetics, currently with a focus on medical applications and on-chip millimeter-wave/THz antennas. He received several awards, including a student paper price at the 2005 IEEE Antennas and Propagation Society International Symposium and the VDE-Promotionspreis 2009 for the dissertation.

Daniel Erni received a diploma degree from the University of Applied Sciences in Rapperswil (HSR) in 1986, and a diploma degree from ETH Zürich in 1990, both in electrical engineering. Since 1990 he has been working at the Laboratory for Electromagnetic Fields and Microwave Electronics, ETH Zürich, where he got his Ph.D. degree in laser physics 1996. From 1995-2006 he has been the founder and head of the Communication Photonics Group at ETH Zürich. Since Oct. 2006 he is a full professor for General and Theoretical Electrical Engineering at the University of Duisburg-Essen, Germany. His current research interests include optical interconnects, nanophotonics, plasmonics, advanced solar cell concepts, optical and electromagnetic metamaterials, RF, mm-wave and THz engineering, biomedical engineering, bioelectromagnetics, marine electromagnetics, computational electromagnetics, multiscale and multiphysics modeling, numerical structural optimization, and science and technology studies (STS). Daniel Erni is a co-founder of the spin-off company airCode on flexible printed RFID technology. He is a Fellow of the Electromagnetics Academy, a member of the Center for Nanointegration Duisburg-Essen (CeNIDE), as well as a member of the Swiss Physical Society (SPS), of the German Physical Society (DPG), of the Optical Society of America (OSA), and of the IEEE.

Ilona Rolfes received the Dipl.Ing. and Dr.Ing. degrees in electrical engineering from Ruhr University Bochum, Bochum, Germany, in 1997 and 2002, respectively. From 1997 to 2005, she was with the High Frequency Measurements Research Group, Ruhr University Bochum, as a Research Assistant. From 2005 to 2009, she was a Junior Professor with the Department of Electrical Engineering, Leibniz University Hannover, Hannover, Germany, where she became the Head of the Institute of Radio frequency and Microwave Engineering in 2006. Since 2010, she has been leading the Institute of Microwave Systems, Ruhr University Bochum. Her research interests include high-frequency measurement methods for vector network analysis, material characterization, noise characterization of microwave devices, sensor principles for radar systems. Dr. Rolfes is currently a member of the Executive Committee of the IEEE MTT-S International Microwave Workshop Series on Advanced Materials and Processes. She is also a Board Member of the German IEEE MTT-AP Chapter and the German Commission for Electromagnetic Metrology of U.R.S.I.

Nils Pohl received the Dipl.-Ing. and Dr.Ing. degrees in electrical engineering from Ruhr University Bochum, Bochum, Germany, in 2005 and 2010, respectively. From 2006 to 2011, he was a Research Assistant with Ruhr University Bochum, where he was involved in integrated circuits for millimeter-wave (mm-wave) radar applications. In 2011, he became an Assistant Professor with Ruhr University Bochum. In 2013, he became the Head of the Department of mm-wave radar and high-frequency sensors with the Fraunhofer Institute for High Frequency Physics and Radar Techniques, Wachtberg, Germany. In 2016, he became a Full Professor of integrated systems with Ruhr University Bochum. He has authored or coauthored more than 200 scientific papers and has issued several patents. His current research interests include ultrawideband mm-wave radar, design, and optimization of mm-wave integrated SiGe circuits and system concepts with frequencies up to 300 GHz and above, and frequency synthesis and antennas. Prof. Pohl is a member of VDE, ITG, EUMA, and URSI. He has received the Karl-Arnold Award of the North Rhine-Westphalian Academy of Sciences, Humanities and the Arts in 2013, and the IEEE MTT Outstanding Young Engineer Award in 2018. He was the co-recipient of the 2009 EEEfCom Innovation Award, the 2012 EuMIC Prize, the 2015 Best Demo Award of the IEEE Radio Wireless Week, the Best Paper Award at EUMIC 2012, the Best Demo Award at RWW 2015, and the Best Student Paper Awards at RadarConf 2020, RWW 2021, and EuMIC 2022.